Optoelectronic and structural characteristics of Er-doped amorphous AlN films

A. R. Zanatta[a] and C. T. M. Ribeiro
Instituto de Física de São Carlos, USP, P.O. Box 369, São Carlos 13560-970, Brazil

U. Jahn
Paul-Drude-Institute für Festkörperelektronik, Berlin 10117, Germany

(Received 14 January 2005; accepted 21 September 2005; published online 7 November 2005)

This work reports on the optical, electronic, and structural properties of aluminum-nitrogen (AlN) films doped with Er. The films were deposited by conventional radio-frequency sputtering at 200 °C in an atmosphere of pure nitrogen. Their main characteristics have been investigated by experimental techniques such as optical transmission, photo- and cathodoluminescence, Raman scattering, and x-ray photoelectron spectroscopy. All films exhibit Er^{3+}-related optical emissions in the visible and infrared regions, which are considerably enhanced after thermal annealing and on measurements at low temperature. Moreover, Raman spectroscopy indicates that the films remain amorphous even after thermal treatment at 900 °C. Based on the composition and on the structural and luminescent properties of these Er-doped amorphous AlN films it was possible to conclude that energy excitation of Er^{3+} ions takes place according to different routes when electrons or photons are used. In the former case, energy is transferred from the amorphous host to the Er^{3+} ions by carrier-mediated processes. As a result, relatively strong Er^{3+}-related optical transitions can be observed in the ~400–1600 nm range. Excitation with 488.0 nm photons also produces visible and infrared Er^{3+}-related luminescence, but most of the optical excitation occurs through direct excitation of the $^4F_{7/2}$ level of Er^{3+}. Finally, the role played by nitrogen atoms and thermal treatments on the achievement of light emission from the present AlN films is discussed and compared with the existing literature. © *2005 American Institute of Physics*.
[DOI: 10.1063/1.2127120]

I. INTRODUCTION

Driven by their great promise in modern technological applications, Er-doped compounds have received widespread attention along the last decades.[1] Such interest relies not only on the possibility to achieve light-emitting materials, but also on the investigation of some of their unique aspects. When triply ionized, Er^{3+} ions exhibit characteristic intra-4*f* optical transitions that, depending on the host matrix, can give rise to infrared, visible, or ultraviolet radiation. Moreover, and because of the partial electronic shielding of the 4*f* orbital by the outer 5*s* and 5*p* shells, the Er^{3+}-related spectral features are almost insensitive to both temperature and local environment. The physical mechanisms behind the excitation of the Er^{3+} ions and their subsequent (optical) recombination, however, are very susceptible to host details such as atomic structure and optical band gap.[2] As a result, various different Er-doped compounds have been extensively investigated towards the achievement of phosphor materials and/or in the development of photonic devices. In both cases the main focus have been the Er^{3+} $^4I_{13/2} \rightarrow {}^4I_{15/2}$ transition at approximately 1540 nm, which coincides with the absorption and dispersion minima of the optical fibers usually employed for telecommunication purposes. In addition to the infrared optical emission at ~1540 nm, Er-doped wide-band-gap (WBG) matrices such as GeN,[3] GaN,[4] SiN,[5] and AlN,[6] for instance, also exhibit visible (or even ultraviolet) radiation and are expected to provide great advances in the development of light-emitting diodes, flat panel displays, etc. As a matter of fact, it is well established that Er^{3+} ions present smaller luminescence quenching when inserted in WBG hosts. This phenomenon is usually attributed to the partial ionic character exhibited by WBG compounds, which influences both the energy and the localization of the electron-hole pairs generated during the process of luminescence excitation.[2]

Hitherto, Er^{3+} ions have been investigated in crystalline[7–10] and amorphous[6,11,12] AlN matrices, following either Er-ion implantation or codeposition. Typically, Er-doped crystalline AlN was obtained from metal-organic molecular-beam epitaxy (MOMBE) with a solid Er effusion source, whereas amorphous AlN was deposited mostly by radio-frequency magnetron sputtering an Al+Er target in a N_2 atmosphere. Based on these experimental efforts important conclusions have been reached: (1) Er^{3+}-related luminescence is substantially enhanced after thermal treatments of crystalline AlN at ~700 °C (Ref. 7) and approximately 1100 °C in *a*-AlN;[6,11,12] (2) either hydrogen or oxygen species influence the Er^{3+}-related luminescence—the former passivating dangling bonds[9] and the latter generating a more favorable environment to the Er^{3+} optical active ions;[10,12] (3) luminescence can take place either after *direct* optical excitation of the intra-4*f* Er^{3+} levels or via *indirect* carrier-mediated processes;[8] and (4) alternating-current thin-film

[a]Electronic mail: zanatta@if.sc.usp.br

electroluminescent (ACTFEL) prototypes have already been obtained from Er-doped *a*-AlN films, clearly indicating the feasibility of optoelectronic devices based on this material.[11]

With the purpose of further investigating the Er-doped aluminum-nitrogen system, this manuscript reports on the optical, electronic, and structural properties of amorphous AlN films deposited by conventional radio-frequency sputtering. After deposition, the films were thermally annealed up to 900 °C and their main characteristics were examined and discussed in close association with the literature.

II. EXPERIMENTAL DETAILS

Er-doped amorphous (*a*-) AlN thin films were prepared by radio-frequency- (13.56 MHz) sputtering a 5-in.-diam target of high-purity (99.999%) aluminum covered at random with small pieces of erbium metal (99.9% pure). The depositions were carried out in a high-vacuum chamber (base pressure $<3\times10^{-6}$ Torr) under an atmosphere of pure nitrogen (2×10^{-3} Torr) and a power density of ~0.8 W cm^{-2}. The *a*-AlN films, typically 0.5 μm thick, were simultaneously deposited onto crystalline-polished silicon (*c*-Si) and quartz substrates kept at ~200 °C. Taking into account the high reactivity of Al to oxygen, and in order to remove eventual contaminants onto the surface of the Al+Er target, each deposition run was preceded by 1 h sputtering with pure argon. After deposition, the films were thermally annealed for cumulative periods of 15 min at 300, 450, 600, 750, and 900 °C under a continuous flow of argon gas. One undoped *a*-AlN film was also deposited and investigated for comparison purposes.

The atomic composition of the as-deposited (AD) films was determined by ion-beam analyses [*Rutherford* backscattering spectrometry (RBS) and nuclear reaction analysis (NRA)] and x-ray photoelectron spectroscopy (XPS). The films were also investigated by optical techniques such as optical transmission in the ultraviolet-visible (UV-VIS) and infrared (IR) regions, Raman-scattering spectroscopy under different photon excitation wavelengths, and photoluminescence (PL), and cathodoluminescence (CL) as a function of temperature.

Room-temperature UV-VIS and IR transmission measurements were performed on commercial spectrophotometers on films deposited onto quartz and *c*-Si substrates, respectively. The Raman analyses were carried out in micro-Raman setups (spot size ~1 μm) with three different excitation sources: 632.8 nm (HeNe laser), 488.0 nm (Ar^+ laser), and 325.0 nm (HeCd laser). Raman measurements were obtained at room temperature, under backscattering geometry, and from films deposited onto c-Si substrates.

All PL measurements employed the 488.0 nm laser line (spot size ~200 μm), a closed cycle He cryostat, and standard *in-phase* detection. In such a case, a nonrefrigerated S-20 photomultiplier tube (PMT) and a liquid-nitrogen-cooled Ge *p-i-n* detector have been used in the 490–850 nm (VIS) and 700–1700 nm (IR) spectral ranges, respectively. The CL data were obtained from a conventional scanning electron microscope (SEM) equipped with an Oxford mono-CL2 and sample cooling facilities. CL signal detection employed either a cooled Si charge-coupled device (CCD) or a cooled InP/InGaAs-based PMT operating in the 200-1100 and 300–1700 nm regions, respectively. During CL experiments an electron beam of 10 keV and 20 nA was adopted rendering analyzed areas of approximately 100×100 μm^2 in films deposited onto polished *c*-Si.

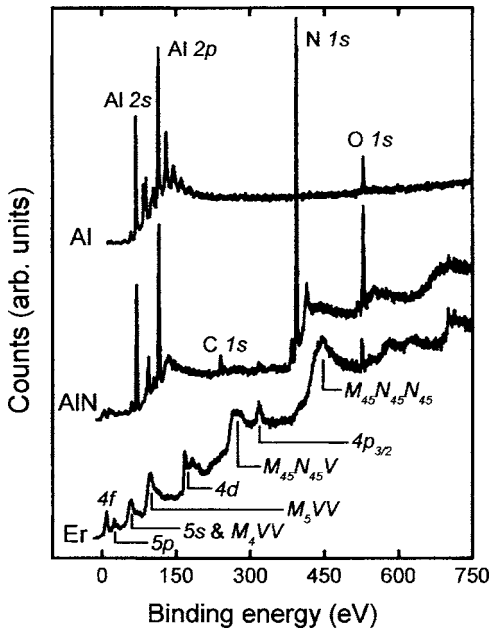

FIG. 1. X-ray photoelectron spectrum of one as-deposited Er-doped amorphous AlN film after Ar^+-ion cleaning (500 eV) for 2 min. The spectra of pure aluminum and Er metal are also shown for comparison. Some of the main photoelectron lines, corresponding either to core levels (Er 4*f* at ~9, Er 5*p* at ~24, Er 5*s* at ~58, Al 2*s* at ~69, Al 2*p* at ~114, Er 4*d* at ~168, C 1*s* at ~285, Er $4p_{3/2}$ at ~318, N 1*s* at ~399, and O 1*s* at ~529 eV) or to Auger transitions (Er M_4VV at ~58, Er M_5VV at ~98, Er $M_{45}N_{45}V$ at ~273, and Er $M_{45}N_{45}N_{45}$ at ~447 eV) are indicated in the figure. The spectra have been vertically shifted for clarity reasons.

The XPS experiments were performed under ultrahigh-vacuum conditions ($\sim10^{-9}$ Torr) with nonmonochromatic 1486.6 eV photons provided by an Al $K\alpha$ x-ray source (energy resolution of typically ~0.8 eV). Since the surface analyses were done *ex situ*, and in order to remove the non-intentional oxygen contamination onto the sample's surface, the films deposited onto *c*-Si substrates were cleaned in high vacuum with energetic (500 eV) argon ions for 2 min prior to each measurement. Ar^+-ion cleaning procedures longer than 2 min seem to produce no change in the XPS spectra.

III. EXPERIMENTAL RESULTS

Both ion-beam analyses and XPS data indicate that the AlN films are almost stoichiometric with $[Al]=(49\pm1)$ at. % and $[N]=(50\pm1)$ at. %. The same applies to the Er-doped samples in which the RBS measurements indicate an Er concentration around 0.5 at. %. Figure 1 displays the XPS survey spectrum of the as-deposited Er-doped AlN film after ion cleaning. The spectra of pure aluminum and Er metal are also shown for comparison. It is clear from Fig. 1 that, even after Ar^+ cleaning, the film presents some superficial oxygen and carbon contamination (<0.5 at. %), which

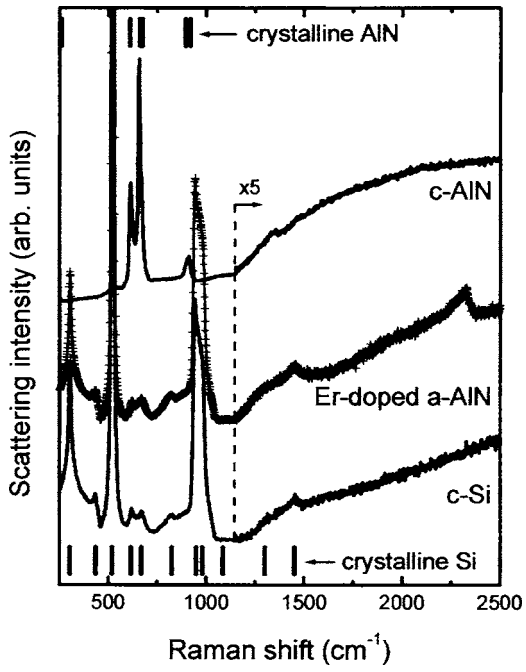

FIG. 2. Raman-scattering spectrum of an Er-doped amorphous AlN film as deposited. The Raman spectra of polycrystalline (*c*-) AlN and Si ⟨111⟩ are also shown for comparison. All spectra have been obtained at room temperature after excitation with a HeNe laser (632.8 nm). They were also vertically shifted for clarity reasons. Notice the multiplying factor for Raman shifts higher than 1150 cm^{-1}. The vertical bars denote the phonon frequencies usually observed in crystalline silicon (bottom of figure) and crystalline AlN (top of figure).

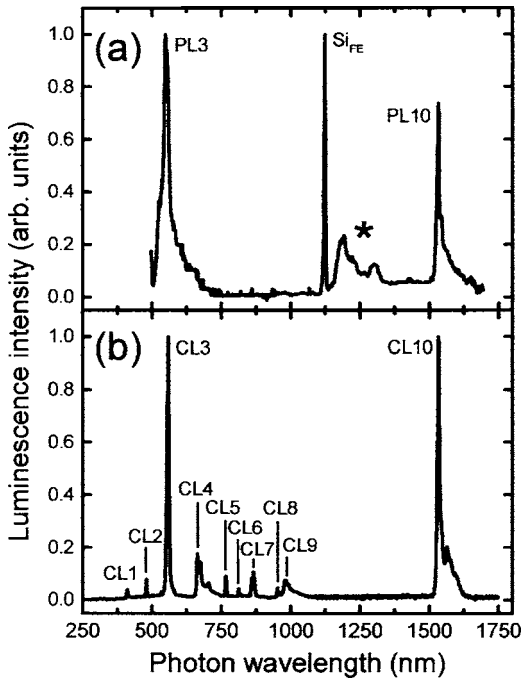

FIG. 3. Luminescence spectra of an Er-doped amorphous AlN film deposited onto *c*-Si. (a) The PL spectrum was obtained at 10 K with 488.0 nm photon excitation (10 mW in a spot size of ~200 μm). (b) The CL spectrum was also obtained at 10 K, from an analyzed area of approximately 100 $\times 100$ μm^2, by using an electron beam of 10 keV (20 nA). Some of the main Er^{3+}-related optical transitions are labeled in the figure. Si_{FE} corresponds to the free-exciton PL signal from the *c*-Si substrate. The star denotes contributions that can be either due to Er^{3+} ions or to the *a*-AlN matrix.

is consistent with the RBS data. Some of the main photoelectron lines[13] (core levels and Auger transitions) were clearly identified in Fig. 1.

In part because of its low content (~0.5 at. %), and especially due to the overlapping of certain photoelectron lines, the presence of Er in the AlN film is not obvious from the XPS spectrum. Based on the intensity of the $4p_{3/2}$ core level, however, the Er concentration was estimated to be in the low (0.3 ± 0.2) at. %, in accord with the RBS measurements. Besides, the absence of Er clustering and of Er–O complexes is clear from the XPS data.

Figure 2 shows the Raman spectrum of the as-deposited Er-doped *a*-AlN film, as obtained with a HeNe laser (632.8 nm). The Raman spectra of a Si ⟨111⟩ substrate and of a polycrystalline AlN target, measured under exactly the same conditions, are also displayed. The vertical bars at the bottom of Fig. 2 denote features relative to crystalline Si and correspond to[14] 2TA(X) at ~304 cm^{-1}, 2TA(Σ) at ~435 cm^{-1}, TO(Γ) at ~520 cm^{-1}, TA(Σ)+TO(Σ) at ~615 cm^{-1}, critical points at ~670 and ~825 cm^{-1}, 2TO(Δ) at ~950 cm^{-1}, 2TO(L) at ~980 cm^{-1}, 2TO(Γ) at ~1085 cm^{-1}, 2TA(X)+2TO(Γ) at ~1300 cm^{-1}, and 3TO(Γ) at ~1450 cm^{-1}. Similarly, the vertical bars at the top of Fig. 2 are related to crystalline AlN (wurtzite structure) and correspond to[15,16] $E_2^{(1)}$ at ~250 cm^{-1}, A_1(TO) at ~610 cm^{-1}, $E_2^{(2)}$ at ~660 cm^{-1}, E_1(TO) at ~675 cm^{-1}, A_1(LO) at ~895 cm^{-1}, and E_1(LO) at ~920 cm^{-1}.

As can be seen from Fig. 2 most of the Raman features observed in the Er-doped *a*-AlN film are due to the *c*-Si substrate. Actually, that is a problem associated with the high transparency of AlN films and, specially, with the low Raman activity of the Al–N dipoles.[17] In any case, the presence of scattered light at ~1260 and 1435 cm^{-1} that are associated with –N=N– groups and/or to aluminum bonded to nonintentional superficial contamination is clear. The signal at ~2295 cm^{-1} is usually attributed to N–Al–N bonds and a relatively narrow signal at ~2330 cm^{-1} corresponds to nonbonded trapped molecular nitrogen and/or to N_2 species adsorbed on the surface of the film.[18,19]

The luminescent properties of the present Er-doped *a*-AlN films were also analyzed either under photon or electron excitation. Figure 3 shows the PL and CL spectra, at 10 K, of the same film deposited onto a *c*-Si substrate. For comparison purposes, and since the total PL (CL) spectrum was obtained with different detectors operating in the UV-VIS and IR ranges, their maximum intensities were normalized. Some of the main PL and CL peaks were labeled in Fig. 3 and their corresponding optical transitions are presented in Table I.[20]

Based on the experimental results of Fig. 3 it is interesting to notice that not all the CL features appear in the PL spectrum, and vice versa. Most of these differences are due to different penetration depths as well as to different mechanisms of energy excitation-recombination.[21,22] Figure 3(a), for example, exhibits a very narrow signal at 1124 nm and some small contributions around 1250 nm. Because of the high transparency of the AlN films at 488 nm, the peak at 1124 nm comes from the crystalline Si substrate and refers

TABLE I. Spectroscopic identification of optical transitions observed in Er-doped *a*-AlN films as obtained from photoluminescence (PL) and cathodoluminescence (CL) measurements at 10 K (Fig. 3). The peak positions are indicated by an average wavelength. GS stands for the ground state ($^4I_{15/2}$) of Er^{3+} ions.

Identification	Optical transition	Peak position (nm)
CL1	$^2H_{9/2} \rightarrow$ GS	410
CL2	$^4F_{7/2} \rightarrow$ GS	480
CL3 (PL3)	$^4S_{3/2} \rightarrow$ GS	560 (550)
CL4	$^4F_{9/2} \rightarrow$ GS	663
CL5	$^2P_{3/2} \rightarrow {}^4S_{3/2}$	766
CL6	$^4I_{9/2} \rightarrow$ GS	810
CL7	$^4S_{3/2} \rightarrow {}^4I_{13/2}$ or $^4I_{9/2} \rightarrow$ GS	858
CL8	$^4F_{7/2} \rightarrow {}^4I_{11/2}$ or $^2P_{3/2} \rightarrow {}^4F_{7/2}$	950
CL9	$^4I_{11/2} \rightarrow$ GS	978
CL10 (PL10)	$^4I_{13/2} \rightarrow$ GS	1532 (1532)

to the phonon-assisted recombination of free excitons (Si_{FE}).[23] The origin of the contributions at approximately 1190, 1220, and 1300 nm, on the contrary, is uncertain. They can be related either to the Er^{3+} ions (corresponding to the $^4F_{9/2} \rightarrow {}^4I_{13/2}$ and $^4S_{3/2} \rightarrow {}^4I_{11/2}$ optical transitions),[20] or they can be attributed to the presence of nitrogen vacancies[24] (V_N) in the amorphous AlN host. Besides, and contrary to the CL spectrum, the broad PL features at ~500–600 nm are a consequence of different excitation-recombination paths, and not because of spectral resolution. Finally, and taking into account the recombination efficiency of rare-earth ions and the high energy of the excitation electrons,[5] the CL spectrum [Fig. 3(b)] presents almost all optical transitions expected from the Er^{3+} ions at low temperature (Table I).[20]

IV. DISCUSSION

Given that the Er concentration stays in the low 0.5 at. %, it is important to mention that both undoped and Er-doped films present almost the same characteristics. At this doping level, Er^{3+} ions are responsible mainly for the development of specific intra-4*f* luminescence either in the VIS or in the IR ranges. As a consequence, all *a*-AlN films exhibit an optical band gap of approximately (5.0±0.3) eV and a very intense IR-absorption band at 680 cm^{-1}. The thermal anneal of the *a*-AlN films, on the contrary, affects not only the luminescent properties of the films, but also their optical band gap and chemical characteristics. As a result of thermal treatments at increasing temperatures the films exhibit changes in the optical-absorption edge, in the Al bonding environment, and in the Er^{3+}-related luminescence intensity.

Figure 4 shows the transmission spectra in the UV-VIS (150–2500 nm) and IR (4000–400 cm^{-1}) ranges of Er-doped *a*-AlN films as deposited and after anneal at 900 °C. As can be seen from Fig. 4(a), thermal annealing (TA) induces a small blueshift and some steepness in the optical-absorption edge. In fact, a similar phenomenon has already been observed in Nd-doped *a*-SiN films and was attributed to the diffusion of atomic nitrogen, to certain structural reordering, or to a combination of them.[25] In addition to changes in the optical characteristics, the influence of thermal annealing on the IR-absorption bands at 680 and 2130 cm^{-1} that are associated with Al–N and AlN–N bonds is evident from Fig. 4(b).[18] Thermal treatments at increasing temperatures seem to promote the diffusion of nitrogen species (and consequent arrangement of the *a*-network) favoring the development of AlN–N bonds. That is shown in the inset of Fig. 4(b) where the ratio between the IR-absorption strength of bands B_1 (AlN–N bonds at 2130 cm^{-1}) and B_2 (Al–N bonds at 680 cm^{-1}) are represented as a function of the annealing temperature.

The PL intensity at ~1540 nm (not shown) scales with the annealing temperature in a way similar to that displayed in the inset of Fig. 4(b) reinforcing the role played by thermal annealing treatments on the optical-electronic characteristics of the present *a*-AlN films. The development of AlN–N bonds and consequent enhancement of the PL signal as a function of the annealing temperature were also observed in Sm-doped *a*-AlN films very similar to those being reported here.[26] In both cases, it seems that an increased number of

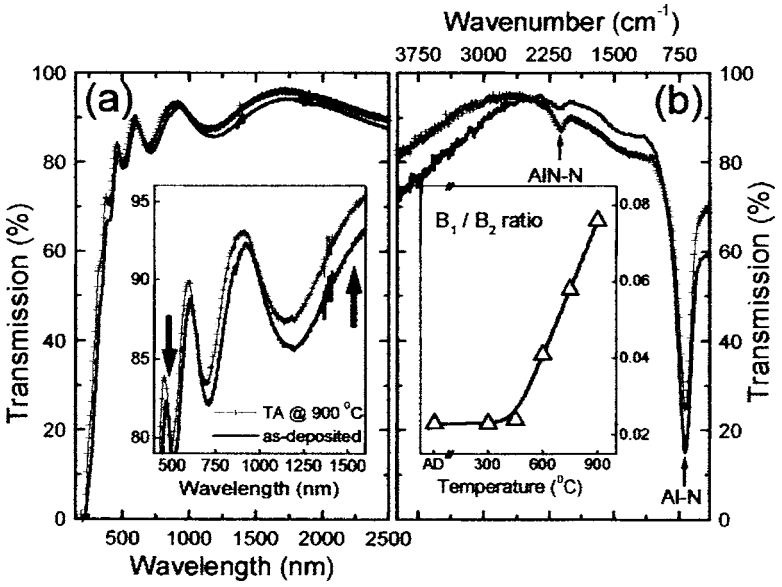

FIG. 4. Optical transmission spectra of Er-doped *a*-AlN films as deposited (black lines) and after thermal anneal (symbols) at 900 °C. (a) UV-VIS-NIR spectra from films deposited onto quartz substrates. The inset shows expanded spectra in the ~450–1600 nm range and indicates the typical transmission values at the wavelength employed during the PL measurements (downward arrow at 488.0 nm) and at ~1540 nm (upward arrow). (b) IR transmission spectra from films deposited onto *c*-Si substrates. As indicated in the figure, Al–N and AlN–N bonds take place at ~680 and 2130 cm^{-1}, respectively. The inset displays the intensity ratio between the absorption bands at 2130 cm^{-1} (B_1 absorption band) and 680 cm^{-1} (B_2 absorption band), as a function of the annealing temperature. TA and AD stand for thermally annealed and as deposited, respectively.

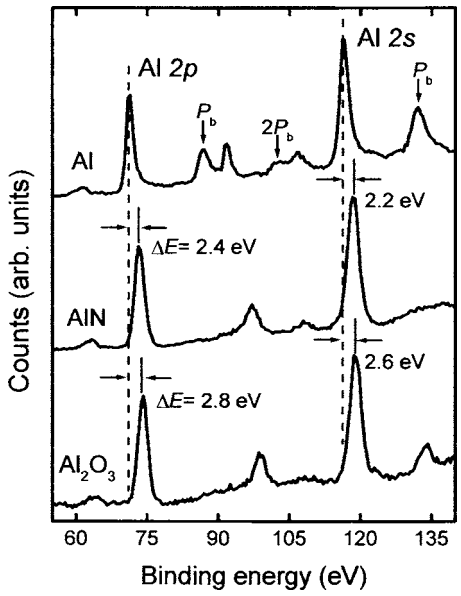

FIG. 5. Detail of the Al 2*p* and Al 2*s* core levels as obtained from XPS measurements of Al metal, amorphous AlN, and sapphire (Al_2O_3). Notice the chemical shift (ΔE) experienced by the Al core levels, as nitrogen (AlN) and oxygen (Al_2O_3) atoms are present. P_b ($2P_b$) stands for the first- (second-) order bulk-plasmon loss features associated with the Al 2*p* and Al 2*s* levels. The spectra have been normalized and vertically shifted for clarity reasons.

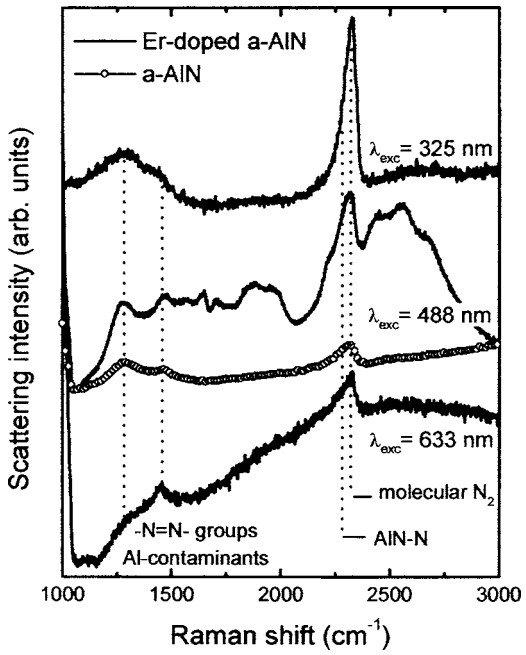

FIG. 6. Room-temperature Raman-scattering spectra of undoped (symbols) and Er-doped AlN (solid lines) films under excitation with 325.0, 488.0, and 638.2 nm photons. Below 1000 cm^{-1}, the Raman features are those corresponding to the crystalline silicon substrate and were not displayed. The spectra were obtained from as-deposited films. The frequency position due to –N═N– (or Al contamination), AlN–N bonds, and molecular N_2 is clearly indicated in the figure. All spectra have been vertically shifted for comparison purposes.

AlN–N bonds provide a favorable chemical environment to the Sm^{3+} or Er^{3+} ions and their consequent optical activation.

As a matter of fact, the existence of impurities in the vicinity of the Er^{3+} ion and/or its insertion in a host with some ionic character seems to be essential for its efficient light emission.[2] For the present *a*-AlN films, and regardless the development of AlN–N bonds, it is important to realize their partial ionic character. Such behavior can be inferred, for example, from photoemission experiments. Figure 5 shows the XPS spectra of Al metal, one amorphous AlN film, and of sapphire (Al_2O_3) in the 55–140 eV binding-energy range. According to Fig. 5, both nitrogen and oxygen atoms induce chemical shifts on the order of ~2–3 eV in the binding energy of the Al 2*p* and Al 2*s* core levels of pure aluminum. The observed chemical shifts, as well as the changes on the energy and intensity of the plasmon loss peaks (P_b and $2P_b$ in Fig. 5), occur mainly because of charge transfer between aluminum and nitrogen (or oxygen in the Al_2O_3 case) species.[13] Likewise, erbium species experience a chemical shift due to the presence of nitrogen. In Er-doped *a*-SiN films, for example, this shift can be as high as 2 eV.[27] As a result, the strong electron affinity of nitrogen may lead to an increased cross section for the Er^{3+} sites, which will act as efficient recombination centers to the existing electron-hole pairs. Alternatively, the high electronegativity of nitrogen can distort (even more) the electrostatic field around Er^{3+} ions and their respective wave functions, with consequent increase in the Er^{3+}-related optical transition probabilities.

The structure of all films considered in this work was investigated by Raman spectroscopy. Considering the very low Raman activity of Al–N bonds, the measurements were performed with photon excitations at 325.0, 488.0, and 632.8 nm. Apparently, the AlN films remain amorphous even after thermal annealing at 900 °C. It does not exclude the existence of micro- or nanostructures inside the AlN films, but certainly they are well below the detection limit of our Raman facilities—either because of the size of the crystalline structures or because of their distribution. Due to the high transparency of the *a*-AlN films [inset of Fig. 4(a)], most of the Raman signal in the ~100–1000 cm^{-1} range comes from the *c*-Si substrate (see Fig. 2). The principal Raman features of the present *a*-AlN films as deposited are shown in Fig. 6. The Raman spectra of *a*-AlN films after thermal treatments exhibit exactly the same phonon features with a substantial enhancement of the mode at ~2300 cm^{-1}, as already observed from the IR transmission data.

The phonon modes related to –N═N– (or Al contaminants) and AlN–N bonds are clear from Fig. 6, as well as some contribution due to molecular nitrogen (superficial or due to enclosed species).[18] The improvement of the Raman signal under UV excitation and the appearance of some Er-related photoluminescence when 488.0 nm photons are used are also evident from Fig. 6. These high-resolution PL features correspond to the Er^{3+} $^4S_{3/2} \rightarrow {}^4I_{15/2}$ (at ~2500 cm^{-1} or 550 nm; PL3 transition in Table I) and $^2H_{11/2} \rightarrow {}^4I_{15/2}$ (at ~1500 cm^{-1} or 525 nm) optical transitions. Whereas the former is very effective at low temperatures [Fig. 3(a)], the latter depends on the thermal population of the $^2H_{11/2}$ level and takes place only at temperatures typically higher than approximately 100 K. At this point it is worthy to remark that PL occurs under 488.0 nm excitation mainly because of the existence of $^4F_{7/2}$ Er^{3+} electronic levels around 20 500 cm^{-1}.[20]

In fact, the quasiresonant optical excitation of rare-earth ions occurs quite often in glasses and has been extensively observed in films such as Sm-doped *a*-AlN,[26] Er-doped *a*-SiN,[5] and Nd-doped *a*-SiN.[25] In all of these cases, and because of the amorphous nature of the solid hosts, the incidence of carrier-mediated excitation mechanisms cannot be discarded, but they certainly are of minor importance when compared with the (quasi-) resonant processes. The high energy provided by electrons during the CL experiments, on the contrary, ensures that all rare-earth ions are being excited via the amorphous matrix by means of hot electrons, for example. Under these circumstances, extra Er^{3+}-related transitions can be observed (see Fig. 3 and Table I) and the luminescence from the amorphous matrix is considerably suppressed.[5]

The luminescence due to the $^2H_{11/2} \rightarrow {}^4I_{15/2}$ (at ~525 nm), $^4S_{3/2} \rightarrow {}^4I_{15/2}$ (at ~550 nm), and $^4I_{13/2} \rightarrow {}^4I_{15/2}$ (at ~1540 nm) transitions has been investigated in detail. For the visible emissions, both PL and CL measurements as a function of temperature indicate a behavior very close to that observed in Er-doped *a*-SiN films.[28] Based on the experimental data our main findings can be summarized as (1) the CL3 emission ($^4S_{3/2} \rightarrow {}^4I_{15/2}$ transition at approximately 550 nm) presents no temperature dependence and its intensity is practically constant in the 10–300 K range; (2) the intensity of PL3, in contrast, starts to drop at temperatures higher than ~150 K because of nonradiative losses; and (3) since the $^2H_{11/2}$ level is thermally populated from the $^4S_{3/2}$ one, the intensity of the $^2H_{11/2} \rightarrow {}^4I_{15/2}$ emission at ~525 nm scales with temperature with almost the same rate in both CL and PL experiments.

Figure 7 shows the infrared PL and CL spectra at room temperature [Fig. 7(a)] and at 10 K [Fig. 7(b)] of one Er-doped *a*-AlN film annealed at 900 °C. Most of the spectral features present in Fig. 7 refer to Stark splitting[29] between the $^4I_{13/2}$ and $^4I_{15/2}$ levels of Er^{3+} ions in the amorphous AlN matrix. While in crystals the Stark manifolds depend on the crystalline structure and symmetry, in amorphous or disordered hosts these features are determined by a combination of different factors. Within them one can mention (i) rare-earth ion concentration, distribution, and eventual clustering; (ii) local electric and magnetic fields (due to compositional nonhomogeneities, for example); (iii) resonant interactions; etc. Therefore, the precise identification of each single spectral feature is not an easy task, especially in amorphous matrices, and requires extensive theoretical and experimental works.[30]

Once excited it is reasonable to expect a very similar recombination route *inside* the Er^{3+} ions. In fact, that seems to be the case if one considers the great resemblance between the spectra obtained after photon and electron excitations (Fig. 7) as well as from the PL(T) and CL(T) behaviors (Fig. 8). In any case, it is not the purpose of this study to identify the different spectral features at ~1540 nm, but to infer about possible excitation paths of the Er^{3+} ions when photons or electrons are used.

As mentioned before both the spectral shape (Fig. 7) and quenching behavior (Fig. 8) of the PL and CL signals at 1532 nm are very similar. Despite these similarities, at least two main aspects call our attention.

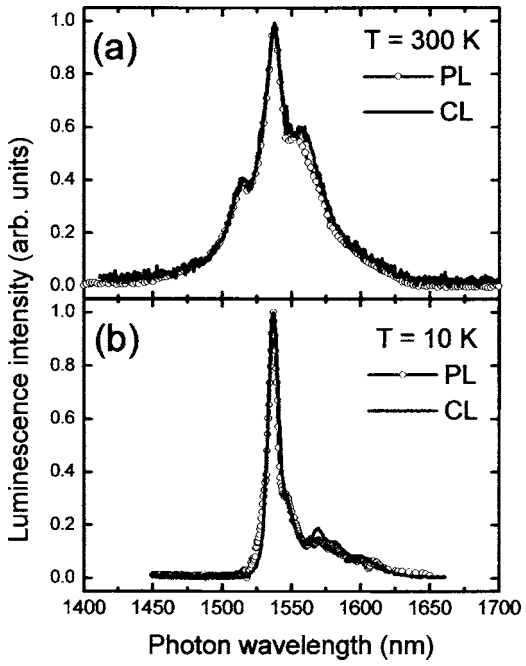

FIG. 7. Photo- (PL) and cathodoluminescence (CL) spectra of an Er-doped *a*-AlN film annealed at 900 °C. The spectra have been achieved at room temperature (a) and at 10 K (b) by means of 488.0 nm photons (PL) or 10 keV electrons (CL). The main feature at 1532 nm corresponds to the $^4I_{13/2} \rightarrow {}^4I_{15/2}$ optical transition due to Er^{3+} ions. The spectra have been normalized for comparison purposes.

(a) Based on the signal-to-noise ratio of all PL and CL data (Fig. 7) and their corresponding temperature-dependent behavior (Fig. 8), the excitation with electrons seems to be much more efficient in producing 1532 nm emission. Notice that, in Fig. 8, the luminescence intensity has been normalized for comparison purposes. Actually, even after normalization, the PL signal at room temperature is one order of magnitude smaller than that exhibited by CL.

(b) The use of either photons or electrons to excite the Er-doped *a*-AlN films yields different optical transitions (Fig. 3). The different intensities obtained from the PL and CL spectra can be attributed to some experimental details such as electron density, laser power, system response, etc. These differences, however, can also have a microscopic origin. The comparative analyses reveal that 10 keV electrons are very effective to supply energy to the *a*-AlN matrix and then to the Er^{3+} ions. The energy transfer (hot electrons → electron-hole pairs) can occur from the conduction band or tail states of *a*-AlN to the Er^{3+} ions (see inset of Fig. 8). Because of its high energy, the electron beam provides enough energy to probe almost all the Er^{3+}-related optical emissions; at the same time it can produce considerable changes on the amorphous network. Compared to crystalline structures, the threshold energy for electron damage in amorphous networks is considerably smaller, namely, about 10^2 keV against 1 keV.[22] More-

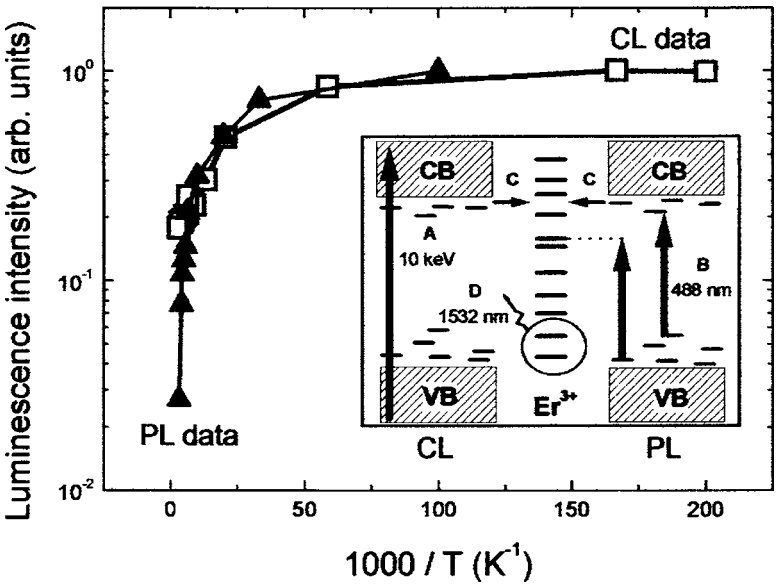

FIG. 8. Temperature-dependent luminescence intensity, as obtained from PL (triangles) and CL (squares) measurements, of the $^4I_{13/2} \rightarrow {}^4I_{15/2}$ optical emission due to Er^{3+} ions in one *a*-AlN film. The data have been normalized for comparison purposes. The inset displays a schematic energy-level diagram and some possible mechanisms that take place after photon (PL) or electron (CL) excitation. VB and CB stand for the valence and conduction bands of *a*-AlN. The following apply: (A) sample excitation with 10 keV electrons, (B) ion (or sample) excitation with 488.0 nm photons, (C) energy transfer from the *a*-AlN CB or tail states to the Er^{3+} ion, and (D) light emission at ~1532 nm after electron recombination between the $^4I_{13/2} \rightarrow {}^4I_{15/2}$ levels.

over, electron irradiation may create defects that are not possible with 488.0 nm photons. These electron-induced defects (mainly broken bonds and atomic displacements) act as nonradiative centers that considerably reduce the luminescence efficiency of the amorphous host resulting in a barely detectable (or no) CL signal. Furthermore, Er^{3+} ions are very efficient recombination centers, which effectively compete with other nonradiative processes present in the *a*-AlN host. As a result, when irradiating the samples with electrons, most of the generated electron-hole (*e-h*) pairs recombine preferentially through the Er^{3+} ions. That could explain the appearance of various Er^{3+}-related optical emissions as well as the absence of CL signal at approximately 1250 nm in Fig. 3.

Optical excitation with 488.0 nm photons, on the other hand, implies a quasiresonant energy transfer to the $^4F_{7/2}$ levels of Er^{3+} ions (inset of Fig. 8). A very small part of this energy can also be absorbed by defects present in the *a*-AlN matrix and give rise to *e-h* pairs. Those *e-h* pairs that do not experience nonradiative transitions can transfer their energy to the Er^{3+} ions. Alternatively, excited Er^{3+} ions can share (or lose) their energy to the amorphous host making the visible PL signal not well resolved and/or inhibiting certain visible optical transitions (Fig. 3). Either the energy loss from *e-h* pairs or from the Er^{3+} ions to the amorphous host can contribute to the development of PL due to nitrogen vacancies V_N, for example. Finally, nonradiative recombination processes, or energy losses to the amorphous host, are at the origin of the almost one order of magnitude decrease in the PL signal at temperatures higher than approximately 150 K (Fig. 8).

V. CONCLUSIONS

In summary, Er-doped amorphous aluminum-nitrogen (*a*-AlN) thin films have been prepared by conventional radio-frequency-sputtering an Al+Er target in an atmosphere of pure nitrogen. After deposition the films were submitted to cumulative thermal treatments and their optical, electronic, and structural characteristics were investigated by means of different spectroscopic techniques. All films exhibit characteristic Er^{3+}-related light emission after excitation with 488.0 nm photons or 10 keV electrons. According to the Raman measurements, the films remain amorphous even after thermal annealing at 900 °C. It is not possible to exclude the existence of small crystallites highly dispersed in the amorphous matrix, but they certainly do not interfere in most of the optical and electronic properties of the films under study. The local environment of the Er^{3+} ions, and consequent luminescence intensity, is greatly influenced by the presence of nitrogen atoms and thermal treatments. According to the experimental data it is reasonable to assume that Er^{3+} ions are excited through carrier-mediated processes when electrons are used. Electron excitation can also induce the development of nonradiative centers, which suppress luminescence from the amorphous host. As a result, the CL signal is typically well resolved with a relatively weak temperature dependence. The excitation of Er^{3+} ions by 488.0 nm photons, on the other hand, occurs mainly by quasiresonant energy transfer to the $^4F_{7/2}$ level. PL and CL spectra display almost the same Er^{3+}-related optical transitions, but PL is highly temperature sensitive because of energy losses to the amorphous host.

ACKNOWLEDGMENTS

The authors are indebted to Professor F. Alvarez (UNICAMP—Brazil) for access to the XPS facilities and to Professor F. L. Freire Jr. (PUC/RJ—Brazil) for the ion-beam analyses. The research group of Professor R. Aroca (University of Windsor—Canada) is also acknowledged for the UV Raman measurements. This work was financially supported by the Brazilian agencies FAPESP and CNPq. The research on rare-earth-doped amorphous semiconductors is part of the CePOF-FAPESP.

[1]For a review on the subject see, for example, A. J. Kenyon, Prog. Quantum Electron. **26**, 225 (2002).

[2]A. R. Zanatta, Appl. Phys. Lett. **82**, 1395 (2003).
[3]A. R. Zanatta and C. T. M. Ribeiro, J. Appl. Phys. **96**, 5977 (2004).
[4]A. J. Steckl and R. Birkhahn, Appl. Phys. Lett. **73**, 2143 (1998).
[5]A. R. Zanatta, C. T. M. Ribeiro, and U. Jahn, Appl. Phys. Lett. **79**, 488 (2001).
[6]K. Gurumurugan, H. Chen, G. R. Harp, W. M. Jadwisienczak, and H. J. Lozykowski, Appl. Phys. Lett. **74**, 3008 (1999).
[7]R. G. Wilson, R. N. Schwartz, C. R. Abernathy, S. J. Pearton, N. Newman, M. Rubin, T. Fu, and J. M. Zavada, Appl. Phys. Lett. **65**, 992 (1994).
[8]X. Wu, U. Hömmerich, J. D. Mackenzie, C. R. Abernathy, S. J. Pearton, R. N. Schwartz, R. G. Wilson, and J. M. Zavada, Appl. Phys. Lett. **70**, 2126 (1997).
[9]S. J. Pearton *et al.*, Appl. Phys. Lett. **71**, 1807 (1997).
[10]A. P. Young, S. H. Gross, L. J. Brillson, J. D. Mackenzie, and C. R. Abernathy, J. Electron. Mater. **29**, 311 (2000).
[11]V. I. Dimitrova, P. G. V. Patten, H. H. Richardson, and M. E. Kordersch, Appl. Phys. Lett. **77**, 478 (2000).
[12]J. C. Oliveira, A. Cavaleiro, M. T. Vieira, L. Brigot, C. Garapon, B. Jacquier, and J. Mugnier, Opt. Mater. (Amsterdam, Neth.) **24**, 321 (2003).
[13]*Practical Surface Analysis*, Auger and X-ray Photoelectron Spectroscopy Vol. 1, edited by B. Briggs and M. P. Seah (Wiley, New York, 1990).
[14]P. A. Temple and C. E. Hathaway, Phys. Rev. B **7**, 3685 (1973).
[15]P. Perlin, A. Polian, and T. Suski, Phys. Rev. B **47**, 2874 (1993).
[16]H. M. Tütüncü and G. P. Srivastava, Phys. Rev. B **62**, 5028 (2000), and references therein.
[17]A. R. Zanatta, C. T. M. Ribeiro, and F. Alvarez, J. Appl. Phys. **92**, 6349 (2002).
[18]C. T. M. Ribeiro, F. Alvarez, and A. R. Zanatta, Appl. Phys. Lett. **81**, 1005 (2002).
[19]See, for example, N. B. Colthup, L. H. Daly, and S. E. Wiberley, *Infrared and Raman Spectroscopy* (Academic, San Diego, 1990).
[20]G. H. Dieke, *Spectra and Energy Levels of Rare-Earth Ions in Crystals* (Wiley Interscience, New York, 1968).
[21]J. I. Pankove, *Optical Processes in Semiconductors* (Dover, New York, 1971).
[22]B. G. Yacobi and D. B. Holt, *Cathodoluminescence Microscopy of Inorganic Solids* (Plenum, New York, 1990).
[23]G. Davies, Phys. Rep. **176**, 83 (1989).
[24]T. L. Tansley and R. J. Egan, Phys. Rev. B **45**, 10942 (1992).
[25]C. T. M. Ribeiro, M. S. Li, and A. R. Zanatta, J. Appl. Phys. **96**, 1068 (2004).
[26]C. T. M. Ribeiro, F. Alvarez, and A. R. Zanatta, Adv. Mater. (Weinheim, Ger.) **14**, 1154 (2002).
[27]A. R. Zanatta, C. T. M. Ribeiro, and F. Alvarez, J. Appl. Phys. **93**, 1948 (2003).
[28]A. R. Zanatta, C. T. M. Ribeiro, and U. Jahn, J. Non-Cryst. Solids **338–340**, 473 (2004).
[29]See, for example, B. Henderson and G. F. Imbusch, *Optical Spectroscopy of Inorganic Solids* (Clarendon, Oxford, 1989).
[30]Q. Wang, N. K. Dutta, and R. Ahrens, J. Appl. Phys. **95**, 4025 (2004), and references therein.